ACS APPLIED MATERIALS & INTERFACES

Research Article

www.acsami.org

One-Pot Self-Assembled Three-Dimensional TiO_2-Graphene Hydrogel with Improved Adsorption Capacities and Photocatalytic and Electrochemical Activities

Zheye Zhang,[†,§] Fei Xiao,[†,§] Yunlong Guo,*[,⊥] Shuai Wang,*[,†,‡] and Yunqi Liu*[,⊥]

[†]School of Chemistry and Chemical Engineering, Huazhong University of Science and Technology, Wuhan, 430074, P. R. China

[‡]State Key Lab of Digital Manufacturing Equipment and Technology, School of Mechanical Science and Engineering, Huazhong University of Science and Technology, Wuhan, 430074, P. R. China

[⊥]Beijing National Laboratory for Molecular Sciences, Institute of Chemistry, Chinese Academy of Sciences, Beijing 100190, P. R. China

Supporting Information

ABSTRACT: We reported the development of a new type of multifunctional titanium dioxide (TiO_2)-graphene nanocomposite hydrogel (TGH) by a facile one-pot hydrothermal approach and explored its environmental and energy applications as photocatalyst, reusable adsorbents, and supercapacitor. During the hydrothermal reaction, the graphene nanosheets and TiO_2 nanoparticles self-assembled into three-dimensional (3D) interconnected networks, in which the spherical nanostructured TiO_2 nanoparticles with uniform size were densely anchored onto the graphene nanosheets. We have shown that the resultant TGH displayed the synergistic effects of the assembled graphene nanosheets and TiO_2 nanoparticles and therefore exhibited a unique collection of physical and chemical properties such as increased adsorption capacities, enhanced photocatalytic activities, and improved electrochemical capacitive performance in comparison with pristine graphene hydrogel and TiO_2 nanoparticles. These features collectively demonstrated the potential of 3D TGH as an attractive macroscopic device for versatile applications in environmental and energy storage issues.

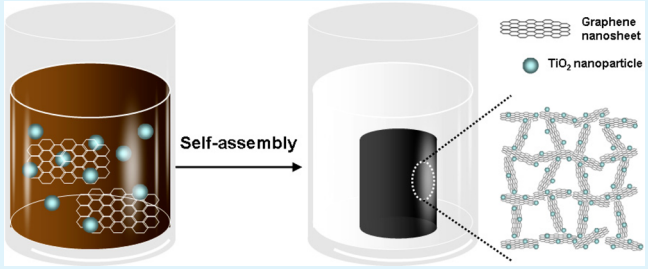

KEYWORDS: *titanium dioxide nanoparticles, graphene hydrogel, self-assembly, photocatalyst, adsorbents, supercapacitor*

1. INTRODUCTION

The integration of nanoscale building blocks into a macroscopic level by the self-assembly method has been recognized as one of the most effective strategies to realize the practical applications of nanomaterials.[1] Nowadays, remarkable progress has been made in self-assembly of nanomaterials into three-dimensional (3D) forms such as hydrogels, aerogels, and some other micropores or mesopores frameworks.[2] Graphene, a single layer of carbon atoms patterned in a hexagonal lattice, has attracted great attention all over the world for its potential applications in catalysis,[3] energy-storage devices,[4] and environmental fields[5] due to its excellent mechanical, electronic, and thermal properties. Previous studies have showed that graphene oxide (GO) can form a 3D hydrogel structure by various supramolecular interactions including hydrogen bonding, coordination, electrostatic interaction, and $\pi-\pi$ stacking.[6,7] Such graphene-based 3D macrostructures are electrically conductive, mechanically strong, and thermally stable. Importantly, recent works have led to the development of functional graphene hydrogels modified with polymers, nobel metals, and metal oxides.[8−12] The resultant graphene-based functional materials with desired structures and properties that take the key advance to realize their extensive potential applications. For example, Yu et al. reported the self-assembly of GO sheets and DNA to form multifunctional hydrogels and found that it possessed high mechanical strength, environmental stability, dye-loading capacity, and self-healing property.[8] Tang et al. demonstrated the controlled assembly of GO into macroscopic porous structures promoted by a noble-metal nanocrystal (Au, Ag, Pd, Ir, Rh, or Pt, etc.); they found that the combination of noble-metal nanocrystals and GO layers resulted in the excellent catalytic activity and selectivity for the Heck reaction.[9] Li et al. also synthesized Au/graphene hydrogel and explored its use for catalytic reduction of 4-nitrophenol.[10] Hou et al. prepared a graphene-polymer hydrogel with reversible volume changes by using environmentally sensitive polymers, poly(N-isopropylacrylamide) (PNIPAAm). The as-obtained hydrogel exhibited high mechanical strength, tunable electrical conductivity, and especially reversible volume changes in response to electric current, making it a potential candidate for artificial muscle devices.[11] Cong et al. developed graphene/α-FeOOH and

Received: January 10, 2013
Accepted: February 17, 2013
Published: February 21, 2013

   dx.doi.org/10.1021/am303299r | ACS Appl. Mater. Interfaces 2013, 5, 2227−2233

magnetic graphene/Fe_3O_4 hydrogels under the synergistic effects of the reduction of GO by ferrous ions and in situ simultaneous deposition of nanoparticles on graphene sheets. Such functional graphene-based hydrogels exhibited excellent capability for removal of pollutants and could be used as capable adsorbents for water purification.[12]

In this work, we demonstrated the development of a new type of multifunctional titanium dioxide (TiO_2) nanoparticles-graphene hydrogel (TGH) by a facile one-step hydrothermal approach and explored its environmental and energy applications as superior photocatalyst, reusable adsorbents, and high-performance supercapacitor. Among a diverse range of semiconductor photocatalysts, TiO_2 nanoparticles have been considered as the most promising materials for widespread environmental applications because of their strong oxidizing power, low cost, relative nontoxicity, long-term thermodynamic stability and photostability, and unique semiconducting properties.[13] Particularly, the composites of TiO_2 nanoparticles and carbon-based materials are currently being recognized as highly effective photocatalysts in the purification of water.[14−16] On the other hand, TiO_2-carbon nanocomposites have also received considerable interest in the electrochemistry field from electrochemical biosensor to supercapacitor because of their excellent chemical stability and electrochemcial activity[17−19] However, the strategy of using TiO_2 nanoparticles and carbon-based materials as multifunctional active materials for both photocatalysts and supercapacitor has not been reported heretofore. Our findings showed that this new type of TGH with 3D interconnected networks and large surface area demonstrated the synergistic effects of the self-assembled TiO_2 nanoparticles and graphene nanosheets. Furthermore, the physical and chemical properties can be greatly improved by optimizing the ratio of TiO_2 nanoparticles and graphene in TGH, enabling it multifunctional for versatile applications in environmental and energy storage issues. When used as adsorbent and catalyst for environmental application, TGH demonstrated high methylene blue (MB) adsorption capacity and photocatalytic activity for degrading MB as well. The maximum adsorption capacity (Q_{max}) of TGH was found to be almost 120 mg g^{-1}, which outperforms many other currently available adsorbents. Meanwhile, the adsorption efficiency of TGH could be effectively recovered by irradiation of the simulated UV light, making TGH reusable for pollutant adsorbent. Furthermore, as an active electrode material for supercapacitor, the as-obtained TGH combined unique pseudocapacity of TiO_2 with high conductivity and electric double layer charging/discharging of graphene and therefore exhibited high specific capacitance (206.7 F g^{-1} at the current density of 0.5 A g^{-1}), acceptable rate capability, and satisfactory cycling stability. These unique properties demonstrate the potential of 3D TGH as an attractive macroscopic device for a wide spectrum of environmental and energy storage applications.

2. EXPERIMENTAL SECTION

2.1. Preparation of Self-Assembled TiO_2-Graphene Hydrogel (TGH). Graphene oxide (GO) was systhesized from graphite powder based on Hummer's method.[20] TGH was prepared by adding a certain amount of TiO_2 nanoparticles (Degussa P25 grade, 20% rutile and 80% anatase) into 2 mg mL^{-1} of homogeneous GO aqueous dispersion (the mass ratio of GO to TiO_2 is in the range from 4:1 to 1:5) under sonication for about 1 h. After that, the mixture was sealed in a 50 mL Teflon-lined autoclave and maintained at 180 °C for 2 h. The autoclave was naturally cooled in room temperature, and then, a black cylinder (i.e., TGH) was obtained. The size of TGH can be freely adjusted by changing the volume of GO aqueous dispersion. 3D graphene hydrogel (GH) was prepared under the same conditions. The as-obtained TGH and GH samples were freeze-dried overnight for the following experiment.

2.2. Characterization. Scanning electron microscopy (SEM) images were obtained on a FESEM instrument (GSM6510LV, JEOL, Japan). The 3D cylinder was scratched off and dispersed in ethanol by sonication. The dispersion was dropped onto a carbon-coated 200 mesh copper grid and dried under room temperature (25 °C) for transmission electron microscopy (TEM) (TECNAI-F20 FEG TEM, Netherlands) observation with an acceleration voltage of 200 kV. Fourier transform infrared (FT−IR) spectra were obtained on Bruker VERTEX 70 FT-IR spectrophotometer (Germany). X-ray photoelectron spectroscopy (XPS) measurements were performed on VG ESCALAB 250 spectrometer with monochromatic Al Kα (1486.71 eV) X-ray radiation (15 kV and 10 mA) and hemispherical electron energy analyzer. X-ray powder diffraction (XRD) patterns were recorded using a diffractometer (X' Pert PRO, Panalytical B.V., Netherlands) equipped with a Cu Kα radiation source (λ = 1.5406 Å). The specific surface area was measured with Micromeritics ASAP2020 Surface Area and Porosity Analyzer and calculated using the Brunauer−Emmett−Teller (BET) equation.

2.3. Dye Adsorption and Photocatalytic Activity Test. Freeze-dried powder of TGH, GH, and TiO_2 nanoparticles were individually dispersed in 5 mL of MB aqueous solution. The amount of TGH, GH, and TiO_2 nanoparticles was chosen as 3.33 mg mL^{-1} in the MB solution for each measure. The suspensions were stirred for 90 min in the dark at room temperature to achieve the adsorption and desorption equilibration. The optical absorption spectra of the samples were obtained using a UV-2550 spectrophotometer (Shimadzu, Japan).

The photodegradation of MB dyes was observed on the basis of the absorption spectroscopic technique. In a typical process, 100 mL of MB aqueous solution (10 ppm) and 40 mg of photocatalysts were placed in a cylindrical quartz vessel. Under stirring, the vessel was exposed to the UV irradiation produced by a 300 W high pressure Hg lamp (the average light intensity was 30 mW cm^{-2}) with the main peak at wavelength of 365 nm. At given intervals, 3 mL of suspension was extracted and then centrifuged at 3000 rpm for 5 min to get rid of the catalysts from the supernatant. Then, the solution was analyzed by recording the UV−vis spectrum of MB at the maximum absorbance of 665 nm.

2.4. Electrochemical Measurement. Cyclic voltammetric (CV), electrochemical impedance spectroscopy (EIS), and chronopotentiometric experiments were performed with a CHI 660 D electrochemical workstation (CH Instruments Inc. US). A conventional three-electrode system was adopted. The as-obtained TGH cylinder was freeze-dried, cut into pieces, and directly used as the working electrode. The counter and reference electrodes were Pt foil and saturated calomel electrode (SCE), respectively. A 0.5 M Na_2SO_4 solution served as electrolyte at room temperature. CV experiments were performed at various scan rates of 5, 10, 20, 50, 100, and 200 mV s^{-1}. Galvanostatic (GV) charge/discharge curves were obtained at various current densities of 0.5, 1, 2, 5, 10, and 20 A g^{-1} to evaluate the specific capacitance.

3. RESULTS AND DISCUSSION

3.1. Characterization of TGH. TGH with well-defined 3D gel-like cylinder can form under different ratio of TiO_2 to graphene in TGH, and the ratio can be freely adjusted in a wide range from 4:1 to 1:5 (Figure 1A inset). Figure 1A shows the SEM image of TGH with the ratio of TiO_2 to graphene 1:5. The as-obtained TGH exhibits well-defined and interconnected 3D porous network with micrometer interconnected pores. From the high magnified SEM image (Figure 1B) and TEM image (Figure 1C), it is found that the pore walls of TGH consist of very thin layers of stacked graphene sheets, where the

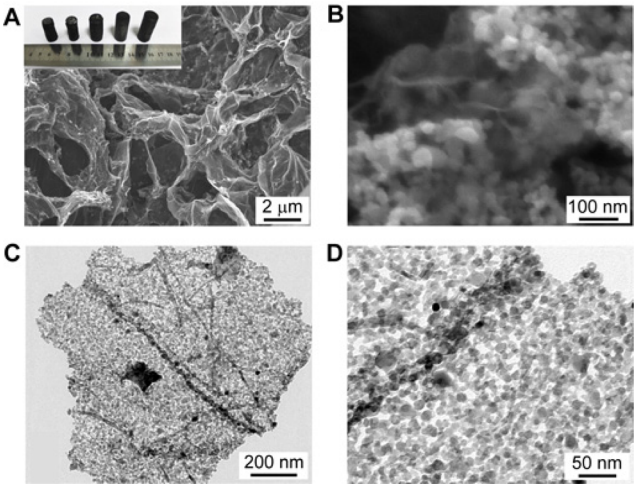

Figure 1. (A, B) Low- and high-magnified SEM images of freeze-dried TGH, inset of (A) is the photograph of TGH with different ratios of TiO_2 to graphene at 180 °C for 2 h (the ratio of TiO_2 to graphene is 4:1, 2:1, 1:1, 1:3, and 1:5 from left to right). (C, D) Low- and high-magnified TEM images of freeze-dried TGH.

spherical nanostructured TiO_2 nanoparticles with uniform size of 20−30 nm were densely anchored onto the graphene nanosheets, and no free or aggregated nanoparticles can be observed from the graphene supports (Figure 1D). Although pristine GO suspension can also be assembled into interconnected 3D framework, graphene sheets tend to aggregate from the formation of hydrogel structure due to the loss in surface oxygen-containing groups after reduction by the hydrothermal process (Figure S1A,B, Supporting Information). The specific surface area of GH (148.58 $m^2\ g^{-1}$) is much smaller than that of TGH (267.98 $m^2\ g^{-1}$, Figure S2, Supporting Information). Therefore, the decoration of TiO_2 nanoparticles on graphene nanosheets not only functionalizes the as-prepared TGH but also acts as the spacer to partially prevent the aggregation of the graphene sheets, which to a great extent increases the specific surface area of TGH. These properties will give priority to potential applications ranging from superior adsorbents to supercapacitors.

FT−IR spectroscopy is used to examine the reduction degree of GO by the hydrothermal process. The spectrum of GO shows the presence of C−O (ν (epoxy or alkoxy)) at 1068 cm^{-1}, C−OH (ν (carboxyl)) at 1396 cm^{-1}, C═C at 1524 cm^{-1}, and C═O in carboxylic acid and carbonyl moieties (ν (carbonyl)) at 1726 cm^{-1}.[21] While for GH the adsorption bands of oxygen functionalities (i.e., C−O at 1068 cm^{-1}, C−OH at 1396 cm^{-1}, and C═O at 1726 cm^{-1}) disappear, only the peak of C═C at 1580 cm^{-1} remains (Figure S3, Supporting Information), indicating the successful reduction of GO via self-assembly by the hydrothermal process. Figure 2A shows the XRD patterns of TGH, GH, and GO samples. For GO sample, the sharp peak at about 2θ = 10.4° is attributed to the (002) reflection of stacked GO sheets, corresponding to an interlayer spacing of 0.83 nm. After the self-assembly process, the sharp peak assigned to the (002) reflection of stacked GO sheets is invisible, and a new broad peak at about 2θ = 24.5° can be seen from GH, which corresponds to an interlayer spacing of 0.36 nm, indicative of the existence of $\pi-\pi$ stacking between graphene sheets that is due to the elimination of oxygenated functional groups on the GH by the hydrothermal process. In the case of TGH, the obvious diffraction peaks assigned as the crystal planes of TiO_2 can be observed. Nevertheless, the dominant peak that is normally observed for graphene sample is imperceptible, revealing a decreased layer-stacking regularity and a highly disordered overlay of individual graphene nanosheets formed in the TGH architecture.

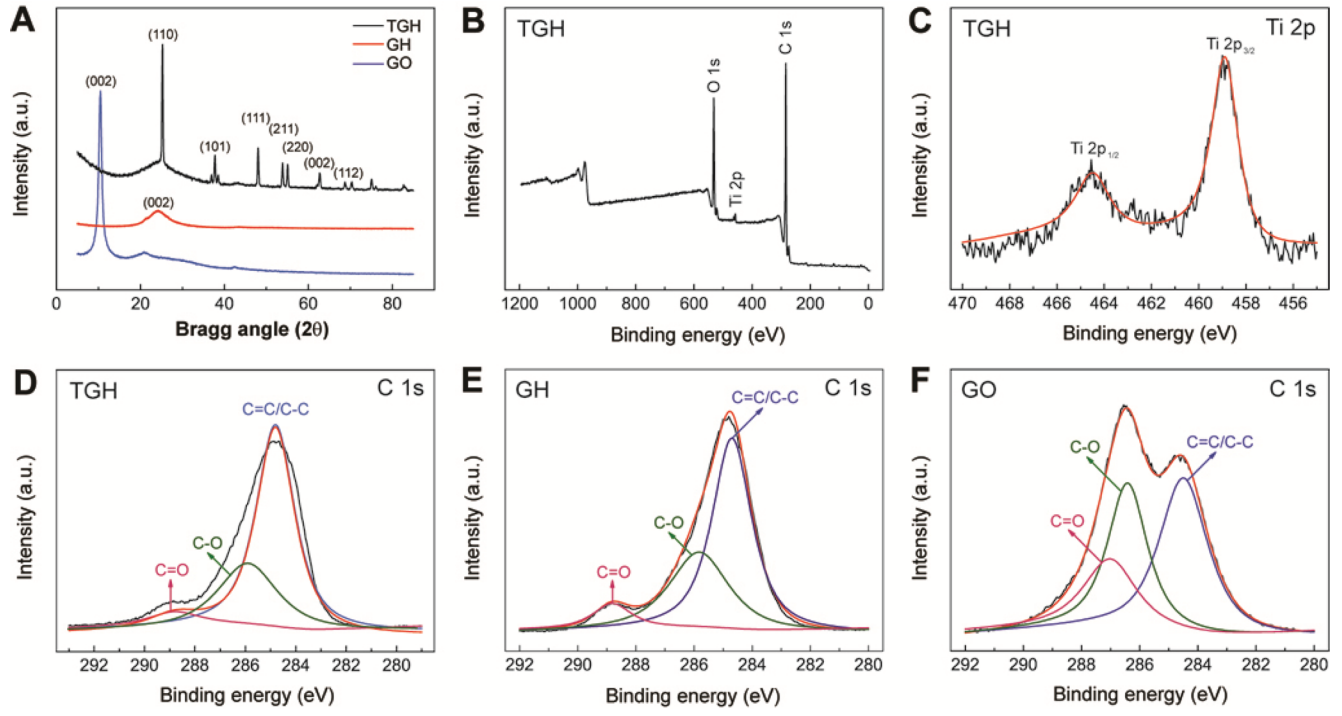

Figure 2. (A) XRD patterns of TGH, GH, and GO. (B) XPS spectra of TGH. (C) Curve fit of Ti 2p spectrum of TGH. (D, E, and F) Curve fits of C 1s spectra of TGH, GH, and GO samples (the ratio of TiO_2 to graphene in TGH is 1:5).

Figure 2B shows the XPS survey spectrum of TGH, where the chemical binding energies located at 284.8, 458.9, and 532.5 eV are assigned to the characteristic peaks of C 1s, Ti 2p, and O 1s, respectively. The core-level XPS signal shown in Figure 2C reveals two peaks at 458.8 and 464.6 eV, respectively, which are in good agreement with the reported XPS data of Ti $2p_{3/2}$ and Ti $2p_{1/2}$ in TiO_2.[22] The curve fit of C 1s spectra of TGH, GH, and original GO are shown in Figure 2D–F. The spectra of both TGH and GH display a predominant peak associated with C═C/C–C (284.8 eV) and a relative weak peak attributed to C–O (286.6 eV), compared to the presence of two main types of carbon bonds of C═C/C–C (284.8 eV) and C–O (286.6 eV) in original GO sample. The significant decreases of the C–O signals in TGH and GH demonstrate a high degree of deoxygenating and successful reduction from GO sample to both GH and TGH during the self-assembly by the hydrothermal process.

3.2. Recoverable Adsorption Capacity and Enhanced Photocatalytic Activity of TGH. The potential application of 3D TGH sample as a reusable organic pollutant scavenger is investigated by chosen MB as model probe. Before measurement, the same amount of TGH, GH, and neat TiO_2 nanoparticles was added into MB dye molecule solutions. After that, all suspensions were stirred for 90 min in the dark to achieve the adsorption and desorption equilibration. The UV–vis optical absorption of TGH, GH, and TiO_2 nanoparticles is shown in Figure 3A. In the presence of TGH, the absorption intensity is almost 3 and 4 times lower than that in the presence of GH and TiO_2 nanoparticles, respectively, revealing that TGH possesses higher dye adsorption capacity in comparison with GH and TiO_2 nanoparticles. The influences of the ratio of TiO_2 to GH in TGH on the adsorption capacity are investigated as well, showing that TGH exhibits the highest adsorption capacity at a optimized ratio of 1:5. The adsorption isotherm of dye molecules as a function of MB concentration on TGH is shown in Figure 3B. The maximum adsorption capacity (Q_{max}) of TGH is found to be almost 120 mg g^{-1},[23] which outperforms many other currently available adsorbents, demonstrating the potential of TGH as a superior adsorbent for practical applications in environmental pollutant management.

The photodegradation of MB is further investigated after MB is adsorbed on the surface of TGH. Figure 4A shows the time

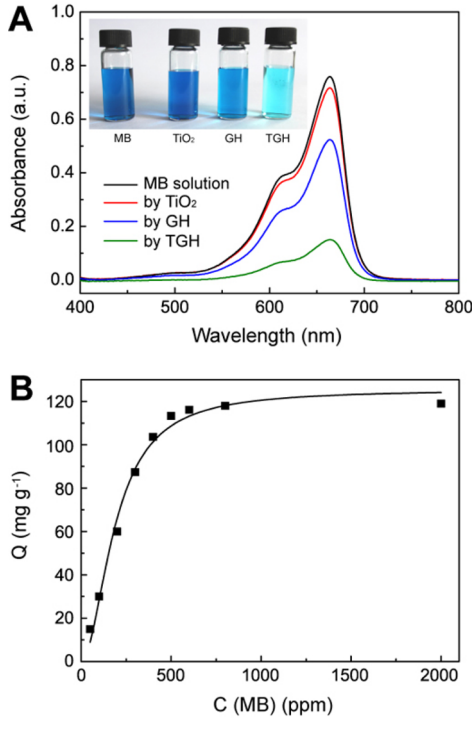

Figure 3. (A) UV–vis absorption spectra of original MB solution, and the adsorptive MB solutions in the presence of TiO_2 nanoparticles, GH, and TGH. Inset is the photograph of orginal MB solution, adsorptive MB solutions in the presence of TiO_2 nanoparticles, GH, and TGH. (B) Dye adsorption isotherms of MB on TGH (the ratio of TiO_2 to graphene in TGH is 1:5, concentration for TGH = 3.33 mg mL^{-1}, $C_{(MB)}$ initial = 50–2000 ppm, T = 298 K).

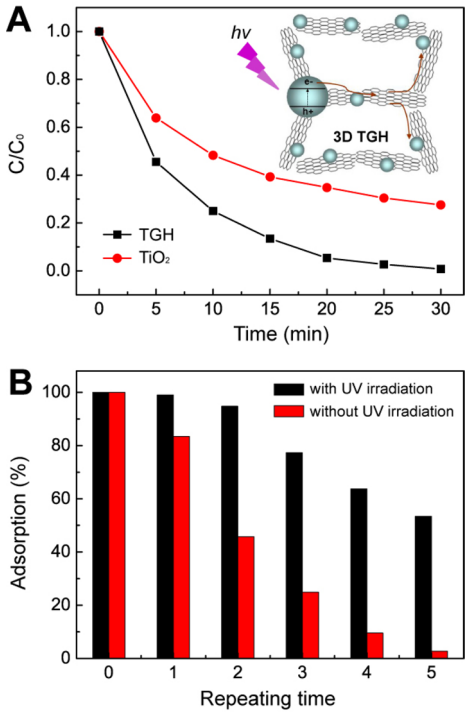

Figure 4. (A) Relative changes of the absorption peak intensity as a function of irradiation time in the presence of TGH and TiO_2 nanoparticles. Inset is the schematic diagrams for illustrating the charge transfer behavior at interfaces in 3D TGH networks. (B) Dye adsorption efficiency of TGH with and without UV irradiation after different sequential cycles (the ratio of TiO_2 to graphene in TGH is 4:1; MB: 10 ppm; TGH: 0.4 mg mL^{-1}).

dependent absorption spectra of MB solutions during simulated UV irradiation in the presence of different photocatalysts. The Y-axis is reported as C/C_0, where C_0 and C are the initial and actual concentration of MB at different reaction times, respectively. In the presence of TGH, the degradation of MB can be completed within 30 min. In contrast, nearly 33% of the initial dye still remains in solution after the same time period for neat TiO_2 nanoparticles (Figure S4, Supporting Information). More importantly, we found that the photocatalytic activities of TGH enhanced with the increase of the ratio of TiO_2 to graphene in TGH and reached the maximum value when the ratio increases to 4:1. The reversibility and regeneration abilities of the TGH have been investigated by performing several adsorption and UV irradiation cycles. In each cycle, simulated UV light was irradiated for 30 min at room temperature. As shown in Figure 4B, 53% of the

dx.doi.org/10.1021/am303299r | ACS Appl. Mater. Interfaces 2013, 5, 2227–2233

photocatalytic activity of TGH still remains after five cycles of photocatalytic reaction. Nevertheless, without irradiation, the adsorption capacity of TGH decreases down to 3% of the original value after five cycles. Therefore, the irradiation of the simulated UV light is effective for the recovery of the adsorption efficiency of TGH, which enables TGH reusable as pollutant adsorbent.

The key advance of TGH with enhanced adsorptivity and better reversibility as well as regeneration should first be assigned to the high adsorption capacity, which is a prequisite for good photocatalytic activity. As mentioned above that 3D TGH sample exhibits large specific area, we believe that the adsorptivity originating from physical adsorption will contribute to the enhancement in the photocatalysis. Furthermore, considering the specific structure of the model organic aromatic pollutant MB, the enhanced adsorptivity should also be attributed to the selective adsorption of the aromatic dye on the aromatic regions of the graphene by $\pi-\pi$ electron coupling.[21,24] In addition, taking into account the chemically bonded TiO_2 nanoparticles and graphene in the 3D netwok of TGH, graphene is recognized as an acceptor of the photogenerated electrons by TiO_2, which expands the light absorption range and ensures fast charge transportation (to suppress the electron−hole recombination) in view of its high conductivity.,[18] Therefore, the electrons could transfer stereoscopically in TGH through the 3D graphene networks,[25] leading to an improvement in photocatalysis of MB by TGH sample.

3.3. Electrochemical Capacitance Properties of TGH.

The electrochemical performance of TGH is evaluated by using it as a working electrode in the supercapacitor system. The optimal ratio of TiO_2 to graphene in TGH is 1:5. The CV curves of TGH electrode at different scan rates are carried out in 0.5 M Na_2SO_4 aqueous electrolyte solution using a three-electrode system (Figure 5A). With potential windows ranging from −0.2 to 0.8 V, the CV curves demonstrate a rectangular and symmetric shape, and no obvious distortion in the curves is observed even at the scan rate of 200 mV s^{-1}, indicative of perfect electrical double-layer capacitance behavior and fast charging/discharging process.[26,27] To explore the advantages of TGH as an ideal electrochemical capacitive electrode, we investigated its CV response with controlled GH carried out at a scan rate of 5 mV s^{-1} (Figure 5B). TGH exhibits better electrochemical capacitive characteristics and superior reversible redox reaction than GH due to the double layer contribution along with the pseudocapacitive contribution. Moreover, as confirmed by the XRD characterization, the intercalation of TiO_2 nanoparticles in TGH could broaden the distance between the graphene nanosheets, which makes it easier for electrolyte ion transfer and is expected to increase the effective surface area and the supercapacitive activity of TGH.

Rate capabilitiy is a crucial parameter to evaluate the power applications of supercapacitors. Figure 6A displays the constant-current GV charge/discharge curves of TGH electode at different current densities. During the charging and discharging steps, the charge curve of TGH exhibits a linear profile, which is almost symmetric to its corresponding discharge counterpart and can be maintained even at a low density of 0.5 A g^{-1} (Figure 6B). Figure 6C shows the variation of specific capacitance of TGH and GH electrodes with an increase in current density. On the basis of the charge/discharge curve, the specific capacitance can be calculated by the equation: $C_t = I\Delta t/m\Delta V$, where I is the discharge current, Δt is the discharge time, m is the mass of the active electrode material, and ΔV is the voltage range of discharge after IR drop.[28−30] The specific capacitance of TGH remains 52% (from 206.7 to 107.0 F g^{-1}) as the current density increases from 0.5 to 10 A g^{-1}. However, the specific capacitance values of GH are not only lower than those of TGH but also decrease significantly with increased current densities (e.g., from 136.2 to 59 F g^{-1} at current density from 0.5 to 10 A g^{-1}), as shown in Figure 6D. The superior rate capability of TGH electrode can be attributed to the synergetic contributions from TiO_2 and graphene interconnected 3D nanostructure, which is in line with the CV results.

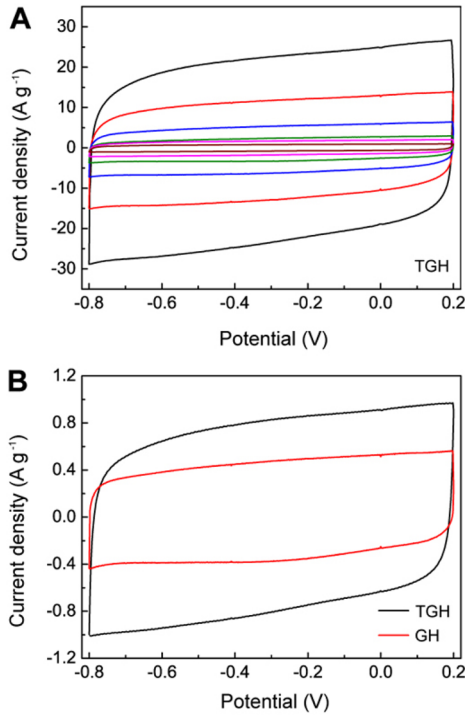

Figure 5. (A) CV curves for TGH electrode at different scan rates (5, 10, 20, 50, 100, and 200 mV s^{-1}) in 0.5 M aqueous Na_2SO_4 electrolyte. (B) CV curves for TGH and GH electrodes at the same scan rate of 5 mV s^{-1}; the ratio of TiO_2 to graphene in TGH is 1:5.

The electrochemical performance of TGH electrode is also investigated by electrochemical impedance spectroscopy (EIS) measurements (Figure 6E). The Nyquist plot of TGH electrode exhibits a small semicircle over the high frequency range; the charge-transfer resistance calculated from the x-intercept on the plot is ∼4.5 Ω. Moreover, TGH has a quite straight line in the low frequency region. The small semicircle observed for TGH electrode indicates small interfacial charge-transfer resistance, whereas the straight vertical line along the series is given rise to ideally polarizable capacitance,[33] which is attributed to a lower diffusion resistance by the shortened proton diffusion path of TGH.

The cycle stability is another important factor in supercapacitor operations. Nonetheless, the cycle life of pseudocapacitive materials such as metal oxides or conducting polymers is always limited because the structure or volume changes during redox reactions lead to the loss of active materials, while the electric double layer capacitors consisting of carbon-based nanomaterials usually show better cycling stability due to the nonexistence of pseudocapacitance effect.[31] Therefore, the incorporation of pseudocapacitive materials into carbon materials is effective to improve the cycle performance of

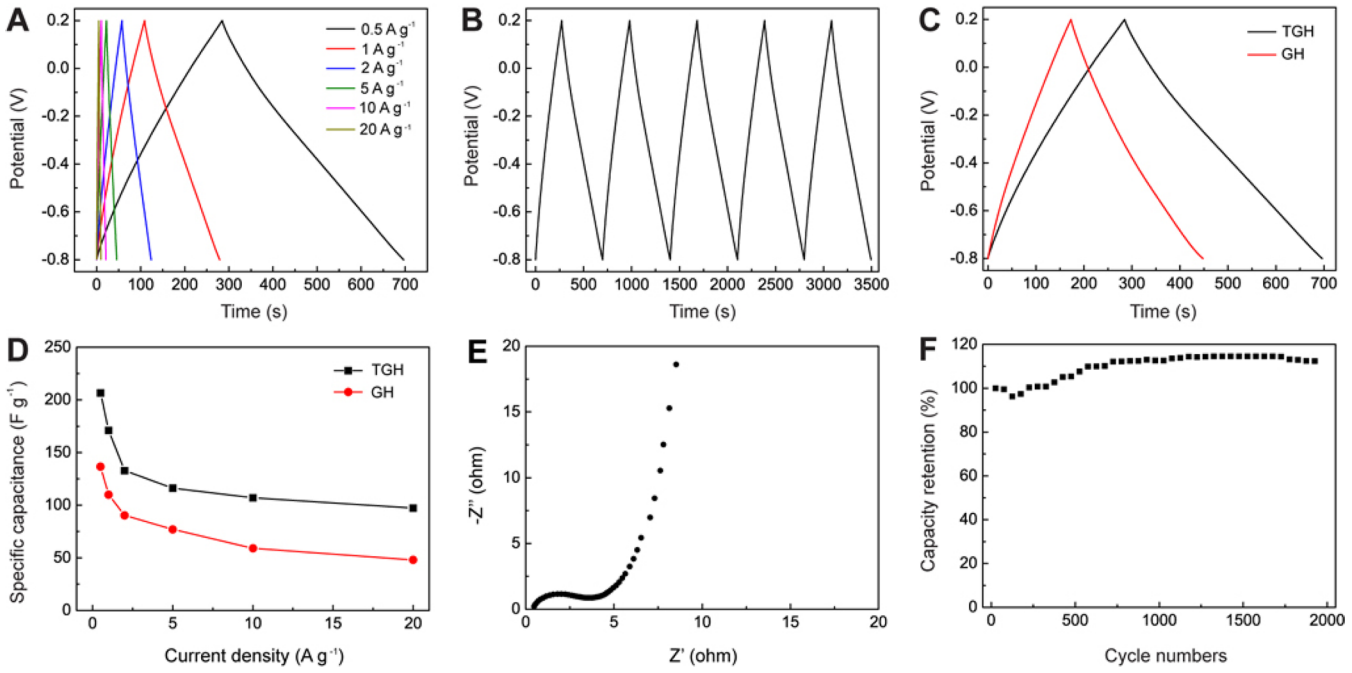

Figure 6. (A) GV charge/discharge curves of TGH electrode at different current densities (0.5–20 A g^{-1}), the ratio of TiO_2 to graphene in TGH is 1:5. (B) GV charge/discharge curve of TGH electrode at the current density of 1 A g^{-1}. (C) GV charge/discharge curves of TGH and GH electrodes at the same current density of 0.5 A g^{-1}. (D) The specific capacitances of TGH and GH electrodes as a function of current densities. (E) EIS curves of TGH electrode. (F) Charge/discharge cycling test of TGH electrode at the current density of 5 A g^{-1}.

supercapacitors. In this study, the cycle stability of the TGH electrode is evaluated by repeating the GV tests in the voltage window from −0.2 to 0.8 V at a current density of 5 A g^{-1}. Due to the pulverization and loss of electrical contact between the active material and the current collector as well as wettability issues,[32] the specific capacitance sharply decreases in the initial 150 cycles (retained ca. 96.4% of its initial capacitance). However, the as-prepared TGH electrode shows well stable capacitance retention over 2000 cycles (Figure 6F). This is because the 3D conductive architecture of graphene hydrygel could serve as both active electrode materials to improve the electrical conductivity and the scaffold to incorporate TiO_2 nanoparticles, consequently enhancing the electrochemical performance and cycling stability significantly.

4. CONCLUSION

In summary, a new type of multifunctional TGH has been fabricated by a facile one-step hydrothermal self-assembled approach. The obtained nanohybrid hydrogel exhibited well-defined interconnected 3D mesoporous microstructure. The spherical nanostructured TiO_2 nanoparticles with a uniform size were densely decorated onto the graphene sheets. The resultant TGH showed the synergistic effects of the self-assembly of graphene sheets and TiO_2 nanoparticles. For recoverable adsorption capacity and photodegradation, the incorporation of TiO_2 nanoparticles and graphene nanosheets not only increased the surface area of the nanohybrid materials but also expanded the light absorption range and enabled fast charge transportation, which enhanced capacity of rapidly adsorbing and photodegrading organic dyes. In addition, for supercapacitor, the combination of the pseudocapacities of metal-oxide and electric double layer charging/discharging properties of graphene in TGH improved the electrochemical performance of active electrode. Therefore, this work is envisioned to open a new way to fabricate multifunctional graphene-based hydrogel and promote their practical applications in environmental and energy storage issues.

■ ASSOCIATED CONTENT

Ⓢ Supporting Information

Supplementary figures. This material is available free of charge via the Internet at http://pubs.acs.org.

■ AUTHOR INFORMATION

Corresponding Author

*E-mail: chmsamuel@mail.hust.edu.cn (S.W.); guoyunlong@iccas.ac.cn (Y.G.); liuyq@iccas.ac.cn (Y.L.).

Author Contributions

§Z.Z. and F.X. contributed equally.

Notes

The authors declare no competing financial interest.

■ ACKNOWLEDGMENTS

This research was supported by National Natural Science Foundation of China (Project No. 51173055).

■ REFERENCES

(1) Man, S. *Nat. Mater.* **2009**, *8*, 781–792.
(2) Gao, Y.; Tang, Z. Y. *Small* **2011**, *7*, 2133–2146.
(3) Li, Y.; Wang, H.; Xie, L.; Liang, Y.; Hong, G.; Dai, H. J. *J. Am. Chem. Soc.* **2011**, *133*, 7296–7299.
(4) Yin, S.; Zhang, Y.; Kong, J.; Zou, C.; Li, C. M.; Lu, X.; Ma, J.; Boey, F. Y. C.; Chen, X. D. *ACS Nano* **2011**, *5*, 3831–3838.
(5) Chandra, V.; Park, J.; Chun, Y.; Lee, J. W.; Hwang, I. C.; Kim, K. S. *ACS Nano* **2010**, *4*, 3979–3986.
(6) Xu, Y. X.; Sheng, K. X.; Li, C.; Shi, G. Q. *ACS Nano* **2010**, *4*, 4324–4330.
(7) Gao, H. C.; Xiao, F.; Ching, C. B.; Duan, H. W. *ACS Appl. Mater. Interfaces* **2012**, *4*, 2801–2807.

(8) Xu, Y. X.; Wu, Q.; Sun, Y. Q.; Bai, H.; Shi, G. Q. *ACS Nano* **2010**, *4*, 7358−7362.
(9) Tang, Z. H.; Shen, S. L.; Zhuang, J.; Wang, X. *Angew. Chem., Int. Ed.* **2010**, *122*, 4707−4711.
(10) Li, J.; Liu, C. Y.; Liu, Y. *J. Mater. Chem.* **2012**, *22*, 8426−8430.
(11) Hou, C. Y.; Zhang, Q. H.; Li, Y. G.; Wang, H. Z. *Carbon* **2012**, *50*, 1959−1965.
(12) Cong, H. P.; Ren, X. C.; Wang, P.; Yu, S. H. *ACS Nano* **2012**, *3*, 2693−2703.
(13) Du, J.; Lai, X. Y.; Yang, N. L.; Zhai, J.; Kisailus, D.; Su, F. B.; Wang, D.; Jiang, L. *ACS Nano* **2011**, *5*, 590−596.
(14) Woan, K.; Pyrgiotakis, G.; Sigmund, W. *Adv. Mater.* **2009**, *21*, 2233−2239.
(15) Zhang, H.; Lv, X. J.; Li, Y. M.; Wang, Y.; Li, J. H. *ACS Nano* **2010**, *4*, 380−386.
(16) Liang, Y. Y.; Wang, H. L.; Casalongue, H. S.; Chen, Z.; Dai, H. J. *Nano Res.* **2010**, *3*, 701−705.
(17) Maryam, S.; Konstantin, K.; Liu, H. K. *J. Mater. Chem.* **2011**, *21*, 5128−5133.
(18) Chen, X. B.; Mao, S. S. *Chem. Rev.* **2007**, *107*, 2891−2959.
(19) Rajeshwara, K.; Osugib, M. E.; Chanmaneec, W.; Chenthamarakshana, C. R.; Zanonib, M. V. B.; Kajitvichyanukuld, P.; Krishnan-Ayera, R. *J. Photochem. Photobiol., C: Photochem. Rev.* **2008**, *9*, 171−192.
(20) Hummers, W. S.; Offeman, R. E. *J. Am. Chem. Soc.* **1958**, *80*, 1339.
(21) Xu, J.; Wang, L.; Zhu, Y. F. *Langmuir* **2012**, *28*, 8418−8425.
(22) Zhang, X. Y.; Li, H. P.; Cui, X. L.; Lin, Y. H. *J. Mater. Chem.* **2010**, *20*, 2801−2086.
(23) Girgis, B. S.; Soliman, A. M.; Fathy, N. A. *Microporous Mesoporous Mater.* **2011**, *142*, 518−525.
(24) Wang, J. F.; Tsuzuki, T.; Tang, B.; Hou, X. L.; Sun, L.; Wang, X. G. *ACS Appl. Mater. Interfaces* **2012**, *4*, 3084−3090.
(25) Hou, C. Y.; Zhang, Q. H.; Li, Y. G.; Wang, H. Z. *J. Hazard. Mater.* **2012**, *205*, 229−235.
(26) Sun, Y. Q.; Wu, Q.; Shi, G. Q. *Phys. Chem. Chem. Phys.* **2011**, *13*, 17249−17254.
(27) Kim, T. Y.; Lee, H. W.; Stoller, M.; Dreyer, D. R.; Bielawski, C. W.; Ruoff, R. S.; Suh, K. S. *ACS Nano* **2011**, *5*, 436−442.
(28) Zhang, J. T.; Jiang, J. W.; Zhao, X. S. *J. Phys. Chem. C* **2011**, *115*, 6448−6454.
(29) Zhang, J. T.; Ma, J.; Zhang, L. L.; Guo, P.; Jiang, J.; Zhao, X. S. *J. Phys. Chem. C* **2010**, *114*, 13608−13613.
(30) Subramanian, V.; Zhu, H.; Vajtai, R.; Ajayan, P. M.; Wei, B. *J. Phys. Chem. B* **2005**, *109*, 20207−20214.
(31) Simon, P.; Gogotsi, Y. *Nat. Mater.* **2008**, *7*, 845−854.
(32) Yan, J.; Fan, Z.; Sun, W.; Ning, G.; Wei, T.; Zhang, Q.; Zhang, R.; Zhi, L.; Wei, F. *Adv. Funct. Mater.* **2012**, *22*, 2632−2641.